JMEPEG
https://doi.org/10.1007/s11665-021-05953-4

1059-9495/$19.00

Microstructure and Mechanical Properties of NiCrMoV Steel Fabricated by Double-Electrode Gas Metal Arc Additive Manufacturing

Wang Xiaowei, Yang Dongqing, Huang Yong, Li Xiaopeng, Wang Lei, and Zhang Guangjun

Submitted: 20 February 2021 / Revised: 19 May 2021 / Accepted: 23 May 2021

Double-electrode gas metal arc additive manufacturing (GMA-AM), capable of reducing heat accumulation through bypass arc, was used to fabricate the thin-wall part of NiCrMoV high-strength low-alloy steel (HSLAS). The peak temperature and cooling time of thermal cycle in double-electrode GMA-AM compared with conventional GMA-AM decreased under the same conditions, which influenced the microstructure and properties of deposited metals. Microstructures of the deposited part were mainly bainite and martensite. As the deposition height increased, the martensite content decreased, and acicular ferrite microstructure was formed due to poor heat dissipation and multiple post-heatments. Introduction of bypass arc into double-electrode GMA-AM generated more martensite structure, which improved the hardness of the deposited part. Tensile strength and yield strength of the thin-wall part were both improved with bypass arc. The average ultimate tensile strength was 855 MPa, and the elongation was 19.5% through double-electrode GMA-AM.

Keywords bypass arc, double-electrode GMA additive manufacturing, microstructure, niCrMoV steel

1. Introduction

Metal additive manufacturing (AM) has attracted increasing attention owing to the expanding industrial demand (Ref 1). The metallic materials fabricated by AM include steels, aluminum alloys, titanium alloys, nickel alloys and precious metals (Ref 2). Metal AM translates feedstock metal materials into compact functional structures through melting and solidification using heat sources such as laser, electron beam and electric arc. The common types of feedstock materials include powder, wires and sheets. Among the available metal AM processes, wire and arc additive manufacturing (WAAM) demonstrates tremendous potential of producing large- or medium-size metal components on account of its simple equipment, low cost and high deposition rate (Ref 3). WAAM can be divided by the difference of electric arc into three main types (Ref 4): gas metal arc AM (GMA-AM), gas tungsten arc AM and plasma arc AM. The latter two types employ tungsten as the electrode of arc, which is non-consumable. In comparison, GMA-AM adopts wire feedstock as the electrode of arc, which is consumable. In GMA-AM, the wire is the anode of arc and directly melts with high speed. Meanwhile, the arc and wire are coaxial, which makes the move of torch more flexible than the other two types. In this respect, GMA-AM is more suitable for fabricating lager metal components at the meter level.

However, droplet transfer is accompanied by enormous amounts of thermal energy during gas metal arc welding (GMAW) to directly enter the molten pool (Ref 5). A similar phenomenon happens in GMA-AM, which further weakens the final forming quality, microstructure and mechanical properties of the part as-built. During fabrication of the thin-wall part by GMA-AM, heat accumulation is worsened as that the deposition height is enlarged (Ref 6). The forming quality of the part fabricated by GMA-AM will be lowered if no effective measure is taken to control heat accumulation. This problem greatly restricts the development and application of GMA-AM.

To eliminate the harmful effect of heat accumulation in GMA-AM, some measures have been proposed, such as control of interlayer temperature, control of transfer mode, change of deposition pattern, online monitoring of deposition size, addition of a magnetic field and the subtractive technology. Spencer et al. introduced an infrared thermometer into GMA-AM to control the layer temperature, which was beneficial for the surface quality and mechanical properties of the deposited components (Ref 7). An effective droplet transition pattern of short circuit with low heat input and little spatter was proposed by Zhang et al. to improve the deposition accuracy of GMA-AM (Ref 8). Ding et al. developed a gap-free path planning method for GMA-AM of thin-wall structures, contributing to deposition quality and material efficiency (Ref 9). The overlapping model for GMA-AM of multi-layer multi-pass parts

This invited article is part of a special topical focus in the *Journal of Materials Engineering and Performance* on Additive Manufacturing. The issue was organized by Dr. William Frazier, Pilgrim Consulting, LLC; Mr. Rick Russell, NASA; Dr. Yan Lu, NIST; Dr. Brandon D. Ribic, America Makes; and Caroline Vail, NSWC Carderock.

Wang Xiaowei, Yang Dongqing, Huang Yong, Li Xiaopeng, and **Wang Lei**, School of Materials Science and Engineering, Nanjing University of Science and Technology, No. 200, Xiaolingwei Street, Nanjing 210094 Jiangsu, China; and Key Laboratory of Controlled Arc Intelligent Additive Manufacturing, Nanjing University of Science and Technology, Nanjing 210094, China; and **Zhang Guangjun**, State Key Laboratory of Advanced Welding and Joining, Harbin Institute of Technology, Harbin 150001, China. Contact e-mail: yangdq@njust.edu.cn.

Published online: 19 August 2021

built by Li et al. improved the final surface flatness and prevented defect formation (Ref 10). Xiong et al. improved the accuracy of deposited width through virtual binocular vision sensing in GMA-AM (Ref 11). Bai et al. introduced an induction coil into GMA-AM to generate the alternating magnetic field, which helped to fabricate structure in non-horizontal positions (Ref 12). Song and Park combined the advantages of WAAM and milling to improve surface quality (Ref 13). These efforts have contributed to the relieving heat accumulation and improving deposition quality, but also decrease deposition rate and undermine the competitiveness of GMA-AM.

In our previous study, double-electrode GMA-AM through introduction of bypass arc was developed to lessen the heat input without weakening the deposition rate, and the forming characteristics including deposited size and material utilization were illustrated (Ref 14). Huang et al. elaborated the effect of bypass arc on metal transfer in bypass-coupled WAAM (Ref 15). The part with excellent formation was fabricated by the optimized metal transfer mode of bridging transfer. However, the microstructure and mechanical properties of components built through double-electrode GMA-AM with bypass arc were not explored, which makes it necessary to investigate the effects of bypass arc on microstructure and mechanical properties.

A NiCrMoV high-strength low alloy steel (HSLAS), which incorporates high-strength into high ductility (Ref 16), was chosen as the test material. This type of steel is increasingly applied in shipbuilding, aircraft, pressure vessels and automotives. Nevertheless, during welding and other hot working processes, the microstructure transformation of this steel is sensitive to heat input. In welding joint of HSLAS, the microstructure of heat-affected zone is also prone to quenching and embrittlement, which limit the practical application of HSLAS. Recently, there is some literature about HSLAS deposited by WAAM. Rodrigues et al. illustrated how the thermal cycle in WAAM acquired by an infrared camera affected the microstructure and mechanical properties of HSLAS structures (Ref 17). Dirisu et al. used two types of wire (ER70S-6 and ER120S-G) to fabricate HSLAS parts by cold metal transfer WAAM (Ref 18) and focused on the fracture toughness and failure mode of the parts as-built. Nemani et al. validated the feasibility of depositing shipbuilding steel (EH36) through WAAM using ER70 feedstock wire (Ref 19). The microstructure evolution and mechanical properties of both the deposited and heat-treated components were characterized. Generally, the HSLAS parts built by WAAM in the existing primary research need to be further optimized (Ref 20).

In this study, NiCrMoV HSLAS was deposited by double-electrode GMA-AM with bypass arc. The thermal cycles of both conventional and double-electrode GMA-AM processes were acquired by infrared thermography. Influence of bypass arc on the microstructure and properties of deposited NiCrMoV HSLAS thin-wall parts was investigated.

2. Experimental Procedures

A double-electrode GMA-AM system with bypass arc was constituted by using a gas metal arc welding (GTAW) torch to complete bypass circuit (I_{bp}) (Fig. 1). The base metal current (I_{bm}) is independent on the melting current (I). The relationship among three currents can be expressed as follows,

$$I = I_{bp} + I_{bm} \quad \text{(Eq 1)}$$

In this condition, a part of the arc energy will flow away through the bypass circuit. Less thermal energy enters the base metal or molten pool, while the wire melting rate, namely melting current, is constant. Two different welding machines were employed as GMA-AM power supply and bypass arc power supply, respectively. The relative locations and distances among two welding torches and the substrate were fixed (Fig. 1). Both torches remained motionless and the thin-wall structures were deposited through horizontal and vertical migration of work flat. The double-electrode GMA-AM system was verified by the collected waveforms of the three currents shown in Fig. 1. The actual currents just satisfy Eq 1.

Surface temperature of the deposited metal was recorded by a thermal infrared camera (Flir SC620). The camera was exactly facing the plane between the electric arc and the deposited thin-wall component. For protection of the lens from the arc radiation and spatter with high temperature, the lens was maintained at a distance of 1 m from the torches. The frame rate for capture was 30 frames/second, and the image resolution was 0.66 mm/pixel.

The feedstock of HSLAS, which was H06MnNi3CrMoA wire in diameter of 1.2 mm, was deposited on the 10Ni5Cr-MoV steel plates in size of 20 × 120 × 250 mm^3. Table 1 illustrates the chemical components of the base metal plate and feedstock wire. A tungsten electrode in diameter of 3.2 mm was employed in the GTAW torch to generate bypass arc. The central deposition parameters are listed in Table 2. The shielding gases for the GMAW torch and the GTAW torch were 95% Ar +5% CO_2 and pure Ar, respectively. The gas flow rates were 15 and 8 L/min, respectively. Two groups of single-pass multi-layer deposition experiments were performed to illustrate the difference between double-electrode GMA-AM and common GMA-AM. Before the experiments, the emissivity for HSLAS was calibrated. The average emissivity of HSLAS was 0.9. In this work, thermal cycles of deposited metals in different GMA-AM processes were elaborated on account of the significant relationship between thermal cycles and microstructure evolution, which further influenced the mechanical properties of the deposited part.

To characterize the microstructure of deposited metals, polished metallographic samples were etched with Nital (4%). Optical microscopic structures at different positions of two deposited parts were inspected using an OLYMPUS GX71 optical microscope. The hardness of the deposited parts along the vertical center line of the samples was measured by an HVS-1000 digital display Vickers hardness tester. Tensile samples with definite sizes, including horizontal and vertical directions (Fig. 2), were cut from the parts as-built. To better compare the tensile properties with or without bypass arc, the sampling location was basically set in the middle region. Re-surfaced tensile specimens were tested under room temperature by a universal testing machine (INSTRON MOBEL1186), with a loading force of 10 kN and a loading speed of 3 mm/min. Elongation and tensile strength were measured after tensile fractures. Meanwhile, the fracture morphology was observed by scanning electron microscopy.

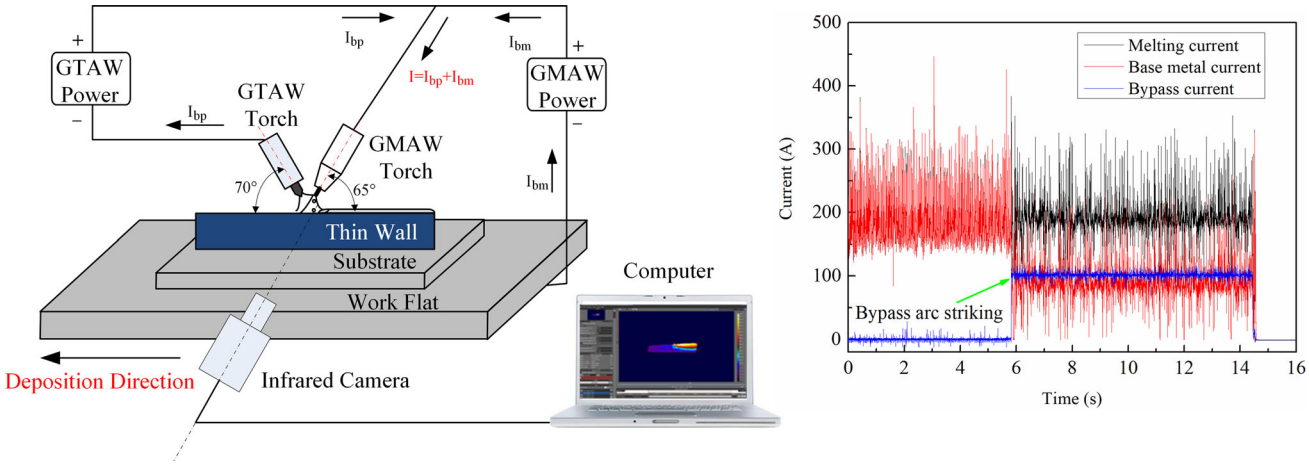

Fig. 1 Schematic diagram of double-electrode GMA-AM system with bypass arc and the collected current waveforms

Table 1 Chemical compositions of substrate and wire (wt.%)

Element	C	Cr	Ni	Mo	V	Si	Mn	S	P	Fe
Substrate	0.07	0.70	4.64	0.40	0.048	0.27	0.56	≤ 0.01	≤ 0.01	Balance
Wire	0.06	0.60	2.50	0.60	0.12	0.30	1.72	≤ 0.01	≤ 0.01	Balance

Table 2 Experimental parameters of double-electrode GMA-AM and GMA-AM

Parameter	Double-electrode GMA-AM	Conventional GMA-AM
Wire feed speed	5 m/min	5 m/min
Arc voltage	23 V	23 V
Bypass current (I_{bp})	90 A	0 A
Traveling speed	5 mm/s	5 mm/s
Inter-layer temperature	120°C	120°C
Deposition height	80 mm	80 mm
Deposition length	160 mm	160 mm

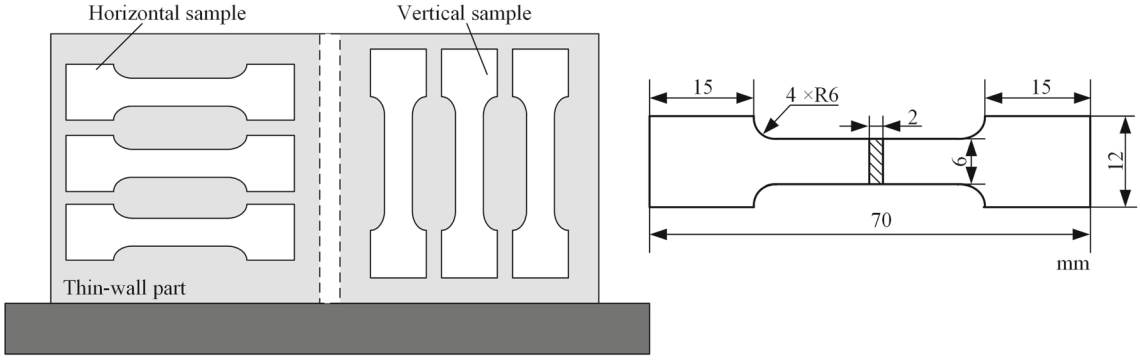

Fig. 2 Cutting location and dimensions of the tensile testing samples

Fig. 3 Macro-profile of final thin-wall parts. (a) Conventional GMA-AM. (b) Double-electrode GMA-AM

3. Results and Discussion

Two thin-wall pares fabricated by double-electrode GMA-AM and conventional GMA-AM, respectively, with satisfactory formation, are presented in Fig. 3. The formation quality of the HSLAS part deposited by conventional GMA-AM outperforms that deposited by double-electrode GMA-AM, which is consistent with the results in Yang et al. (Ref 14). On the cross-sections of deposition metals, there is no obvious defect in either part. The metallographic specimens of deposited components are mainly organized into three segments: top, middle and bottom regions (Fig. 3). The thermal cycle, microstructure and mechanical properties of the deposited parts will be elaborated below.

3.1 Thermal Cycle of Deposition Process

Typical thermal cycle curve including heating rate, peak temperature, cooling rate crucially influences the microstructure evolution of deposited components, which in turn impact the mechanical properties. This section focuses on the thermal cycle of deposited metals during single-pass multi-layer deposition and presents crucial information such as peak temperature and cooling rate. In general, cooling rates can be condensed into the time periods of temperature drop from 800 to 500°C ($t_{8/5}$) and from 800 to 300°C ($t_{8/3}$).

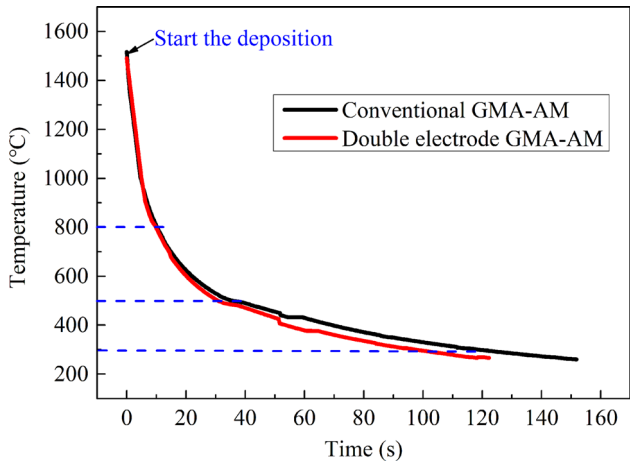

Fig. 4 Thermal cycle of deposited metal in top region for conventional GMA-AM process and double-electrode GMA-AM process

In the top region (the last layer), metals only suffer one thermal cycle, and the cooling rate in double-electrode GMA-AM is faster than that of conventional GMA-AM (Fig. 4). The $t_{8/5}$ and $t_{8/3}$ of GMA-AM are 20.0 and 87.4 s, respectively, with bypass arc, but are 23.6 and 110.2 s, respectively, without

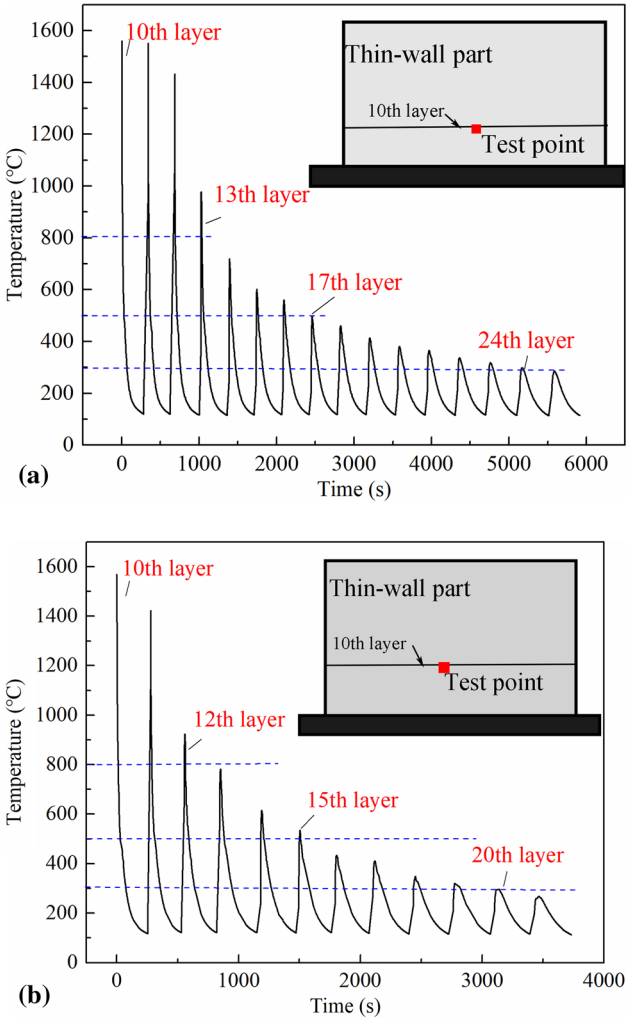

Fig. 5 Thermal cycles of the 10th layer deposition metal with different bypass current. (a) GMA-AM process and (b) Double-electrode GMA-AM process

bypass arc. In the middle region, metals experience multiple thermal cycles. For simplification of analysis, the thermal process of deposited metals on the 10th layer was chosen. The typical thermal cycling curves for deposited metals at this layer are obviously different between conventional GMA-AM and double-electrode GMA-AM (Fig. 5). The deposited metals at this layer undergo multiple remelting and post-heating cycles in the subsequent deposition, which affect the final microstructure and performance of components. For conventional GMA-AM, the deposited metals in the 10th layer after solidification and cooling will remelt during deposition of the 11th and 12th layers, because the peak temperature of the test point exceeds the melting point of 1450°C (Fig. 5a). With the use of 90 A bypass current, the deposited metals of the 10th layer will only remelt during the deposition of the 11th layer (Fig. 5b).

The peak temperature of deposited metals at the middle of the 10th layer during the subsequent depositions is also higher in conventional GMA-AM (Fig. 6). With the absence of bypass

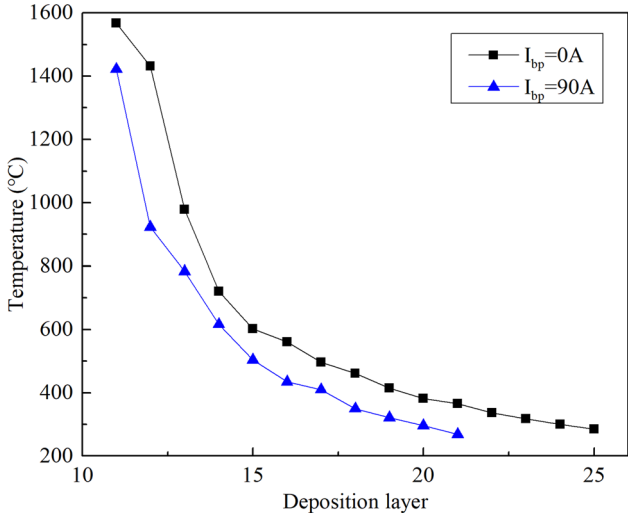

Fig. 6 Peak temperature of the 10th deposition metal with different bypass current

Table 3 The span of $t_{8/5}$ and $t_{8/3}$ of the 10th layer's deposition metal with different bypass current

	$t_{8/5}$		$t_{8/3}$	
Layer number	**I_{bp}= 0 A**	**I_{bp}= 90 A**	**I_{bp}= 0 A**	**I_{bp}= 90 A**
10th	18.7 s	17.8 s	56.3 s	64 s
11th	19.3 s	21 s	60.4 s	70.9 s
12th	21.2 s	22.4 s	64.5 s	75.3 s
13th	27.2 s	…	83.7 s	…

arc, the peak temperature of deposited metals at the 10th layer is below 300°C until the deposition of the 25th layer. With the bypass current of 90 A, for deposited metals at the 10th layer, the post-heat peak temperature is less than 300°C in the deposition of 21st layer. As deposition layer number increases, the peak temperature of deposited metals in the 10th layer gradually drops. With bypass current of 90 A, the peak temperature corresponding to the same deposition layer number is lower than the case without bypass current. Under the same deposition rate and interlayer temperature, introduction of bypass arc relieves the thermal effect on the deposited metal in GMA-AM, which is beneficial for the properties of the part as-built. Table 3 shows $t_{8/5}$ and $t_{8/3}$ of the 10th layer deposited metals through the thermal cycle in subsequent deposition. From the 10 to 12th layers, $t_{8/5}$ and $t_{8/3}$ are slightly longer in double-electrode GMA-AM. However, with the absence of bypass arc, the deposition of the 13th layer greatly influences the cooling of the 10th layer deposited metals, which moderately prolongs $t_{8/5}$ and $t_{8/3}$. After the introduction of bypass arc, the temperature of deposited metals does not exceed 800°C in the deposition of the 13th layer (Fig. 5b), which little influences the $t_{8/5}$ and $t_{8/3}$ of the 10th layer. Therefore, the eventual $t_{8/5}$ and $t_{8/3}$ are longer in GMA-AM. This change can be attributed to

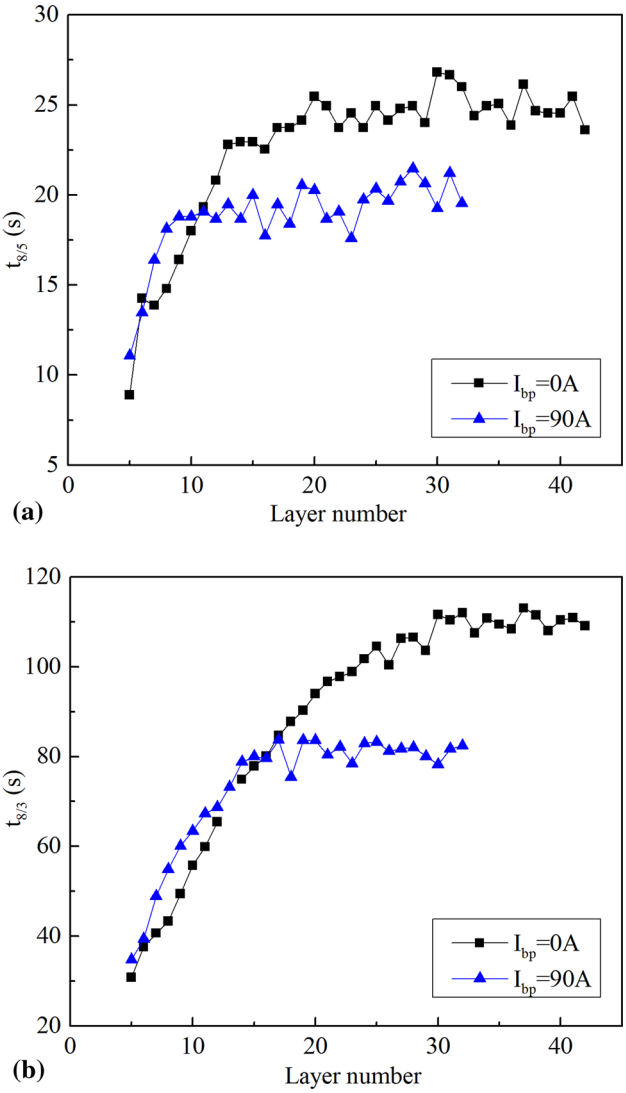

Fig. 7 Spans of (a) $t_{8/5}$ and (b) $t_{8/3}$ of each layer with different bypass currents

the reduction of thermal energy input through the bypass arc. The thermal cycles of other layers have similar indication except for the difference of extent. The spans of $t_{8/5}$ and $t_{8/3}$ in the deposition of each current layer are prolonged gradually from the 5th to the 15th layers (Fig. 7). The $t_{8/5}$ and $t_{8/3}$ after the deposition of the 15th layer increase slowly with minor fluctuations. For double-electrode GMA-AM with bypass arc of 90 A current, $t_{8/5}$ and $t_{8/3}$ are about 6 and 30 seconds, respectively, which are shorter than those of conventional GMA-AM.

All above results indicate that for double-electrode GMA-AM with bypass arc, the temperature of deposited metals drops faster compared with conventional GMA-AM. Under the same conditions, the peak temperature of deposited metals is lower, and the cooling time of $t_{8/3}$ and $t_{8/5}$ is shorter in double-electrode GMA-AM with bypass arc. The particular thermal behavior will considerably impact the microstructure and mechanical properties of deposited components.

3.2 Microstructure

During GMA-AM, the deposited metals in different positions experience different thermal processes. The microstructure of the thin-wall part is nonuniform along the direction of built height. Figure 8 illustrates the microstructure of thin-wall parts deposited by conventional GMA-AM and double-electrode GMA-AM with bypass arc. In the top region, the deposited metal does not go through post-heat treatment compared with the metals in the middle and bottom regions. Bainite and lath martensite are formed in the top region after deposition (Fig. 8a and b). Due to the faster cooling speed in double-electrode GMA-AM with bypass arc, there is more martensite in the top region (Fig. 8b). Based on the reported continuous cooling transformation (CCT) diagram of this NiCrMoV steel (Ref 21) (Fig. 9), the critical cooling rate $t_{8/3}$ for martensite transformation is less than 100 s. For double-electrode GMA-AM with cooling rate $t_{8/3}$ of 87 s, there is partial martensite microstructure. For GMA-AM with cooling rate $t_{8/3}$ of 110.2 s, there is no martensite microstructure. These results are consistent with the metallographic examination.

In the middle region, the deposited metal experienced several cycles of post-heat treatment. The microstructure in this region is obviously different between double-electrode GMA-AM and conventional GMA-AM. The major microstructure of the middle region for conventional GMA-AM is composed of acicular ferrite and granular bainite, with little martensite (Fig. 8c). For double-electrode GMA-AM, the lath martensite still appears in the middle region, accompanied with abundant granular bainite and a fraction of ferrite (Fig. 8d). The thermal cycle of the deposited metals crucially influences the microstructure transformation. Compared with the microstructure of the top region, finer grain size can be obtained in the middle region after multiple heating cycles. The deposited metals in the bottom region also endured several times of post-heat treatment. However, heat dissipation in the bottom region was better due to the shorter distance to the substrate, which was conducive to heat conduction and quickened the cooling rate. It is deduced that more martensite and less ferrite microstructure are formed in this region. Despite multiple post-heat cycles, a fraction of martensite and bainite microstructure remains in the bottom region (Fig. 8e and f). Therefore, with the increase of deposition height, the microstructure of deposited parts changes from abundant bainite and martensite to ferrite and bainite. For double-electrode GMA-AM with bypass arc, more martensite structure is generated in the deposited part. The formation of ferrite does not accord closely with the CCT diagram of NiCrMoV steel. The chief cause is the multiple heating cycles after deposition in the middle region. The subsequent heat-treatment accounts for the formation of more acicular ferrite (Ref 22).

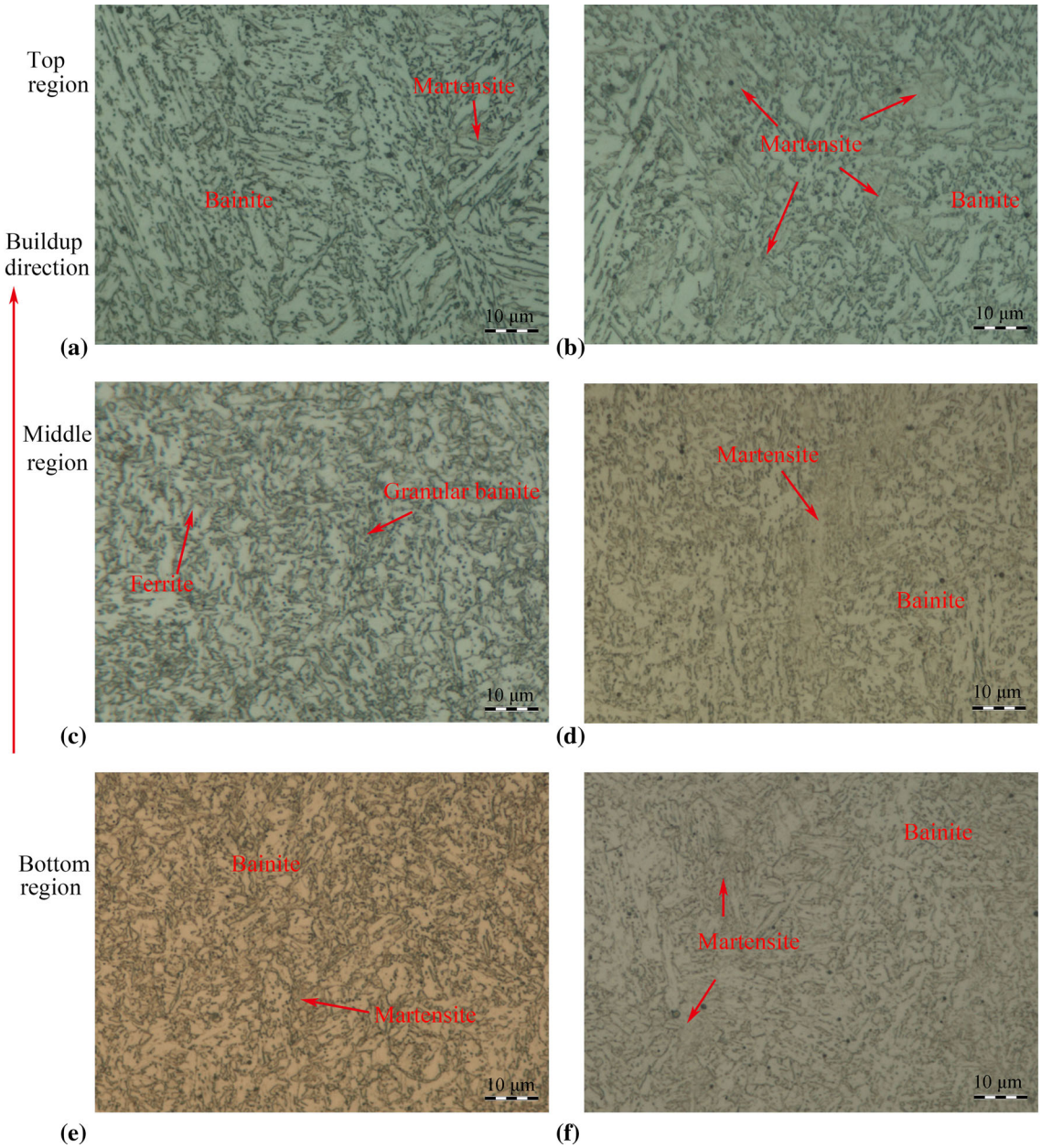

Fig. 8 Microstructure of deposited parts. (a) Top, (c) middle and (e) bottom regions of conventional GMA-AM. (b) Top, (d) middle and (f) bottom regions of double-electrode GMA-AM with bypass arc

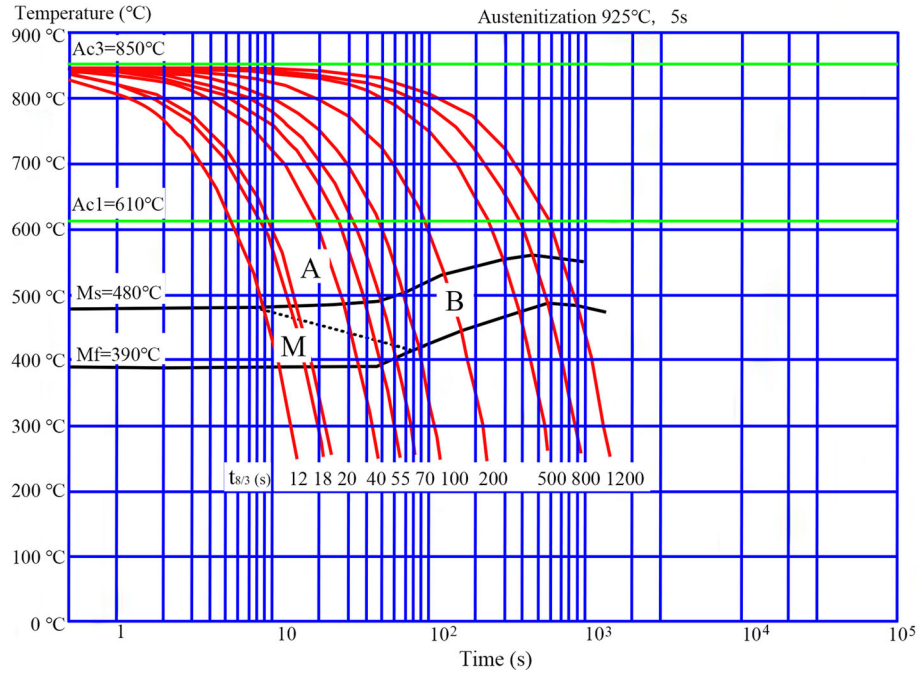

Fig. 9 Continuous cooling transformation diagram of NiCrMoV steel from Li et al. (Ref 21)

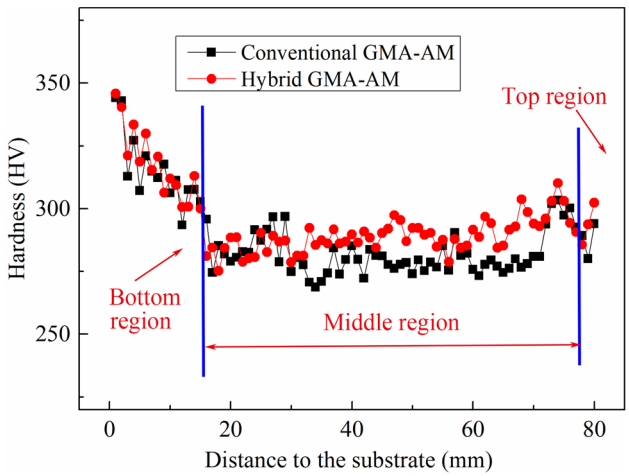

Fig. 10 Microhardness of the deposited parts

3.3 Mechanical Properties

3.3.1 Microhardness. Figure 10 presents the microhardness of the deposited parts. For the two deposited parts, the hardness firstly decreases with the increment of deposition height, and then remains unchanged on the whole. The reason for this variation is the difference of microstructure. In the bottom region, the existence of martensite and bainite improves the hardness. As the buildup height is enlarged, the martensite amount decreases, and ferrite is formed as a result of slow cooing rate caused by poor heat dissipation. The variation trends and values of microhardness are generally consistent between GMA-AM processes. The mean microhardness of the deposited component by double-electrode GMA-AM with bypass arc is 315.6, 289.4 and 293.9 HV from the bottom to top regions, respectively. The corresponding results of conventional GMA-AM are 314.0, 280.2 and 286.8 HV, respectively. The major difference between GMA-AM processes lies in the value of the middle region. According to previous analysis of microstructure, more martensite structure was generated in the middle and top sections of the part fabricated by double-electrode GMA-AM with bypass arc. After subsequent deposition, the hardness of the deposited metal will be improved for the GMA-AM with bypass arc.

3.3.2 Tensile Properties. Figure 11 shows the results of tensile testing of the horizontal and vertical samples for deposited parts with different bypass currents, including the ultimate tensile strength (UTS), yield strength (YS) and elongation. Generally, the values of tensile properties are higher in the deposited component by double-electrode GMA-AM with bypass arc of I_{bp} = 90 A, and the horizontal samples outperform the vertical samples. The mean UTS of HSLAS deposited by double-electrode GMA-AM is 855 MPa (horizontal) and 830 MPa (vertical), which are about 50 and 40 MPa higher compared with GMA-AM without bypass arc, respectively (Fig. 9a). With bypass arc of 90 A, the mean YS of HSLAS components is 789 MPa (horizontal) and 687 MPa (vertical). These data are significantly higher compared with the HSLAS components by conventional GMA-AM, which are only 650 and 628 MPa, respectively. With bypass arc, the strength of deposited metals is higher due to the richer amount of martensite structure. The elongation to fracture of both deposited HSLAS parts changed little. The elongation rates of horizontal and vertical samples are 19.5 and 18.4%, respectively, for double-electrode GMA-AM and are 18.2 and 16.7%, respectively, for conventional GMA-AM. The typical stress-strain curves demonstrate the ductility of deposited metals is largely consistent among different bypass currents (Fig. 11d). Figure 12 shows fracture morphology of tensile test samples. The macroscopic section of fracture indicates the obvious characteristics of ductile fracture (Fig. 12). Numerous dimples

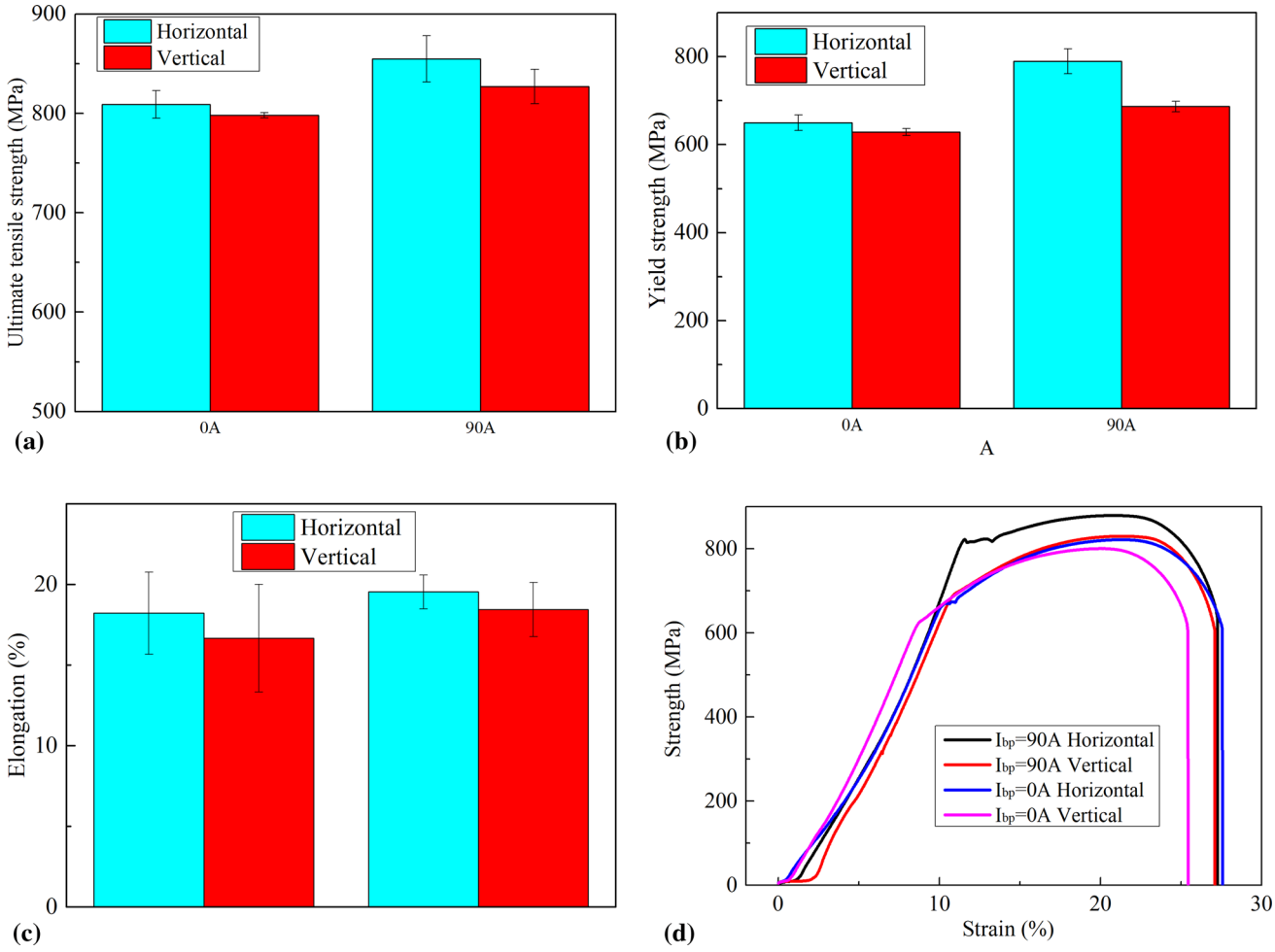

Fig. 11 Tensile test results of deposited parts fabricated by conventional GMA-AM and double-electrode GMA-AM. (a) Ultimate tensile strength. (b) Yield strength. (c) Elongation. (d) Stress-strain curves

were observed on the fracture surface. From the perspective of crack propagation, the fracture is transgranular, and the corresponding fracture mechanism is ductile transgranular fracture of microvoid coalescence.

4. Conclusions

- NiCrMoV HSLAS steel deposited by double-electrode GMA-AM with bypass arc and conventional GMA-AM exhibits a well-formed appearance.
- With bypass arc, the cooling time of $t_{8/5}$ and $t_{8/3}$ is shortened. The peak temperature of deposited metals is lower in GMA-AM under the same conditions.
- The deposited NiCrMoV steel is mainly composed of bainite and martensite. With bypass arc, the amount of martensite structure in deposited metals increases. Without bypass arc, the subsequent heat-treatment leads to the formation of acicular ferrite.
- The NiCrMoV steel fabricated by double-electrode GMA-AM with bypass arc demonstrates higher yield strength of 789 MPa, ultimate tensile strength of 855 MPa and higher microhardness compared with conventional GMA-AM. The elongation of deposited parts similar and approaches 16–20%.

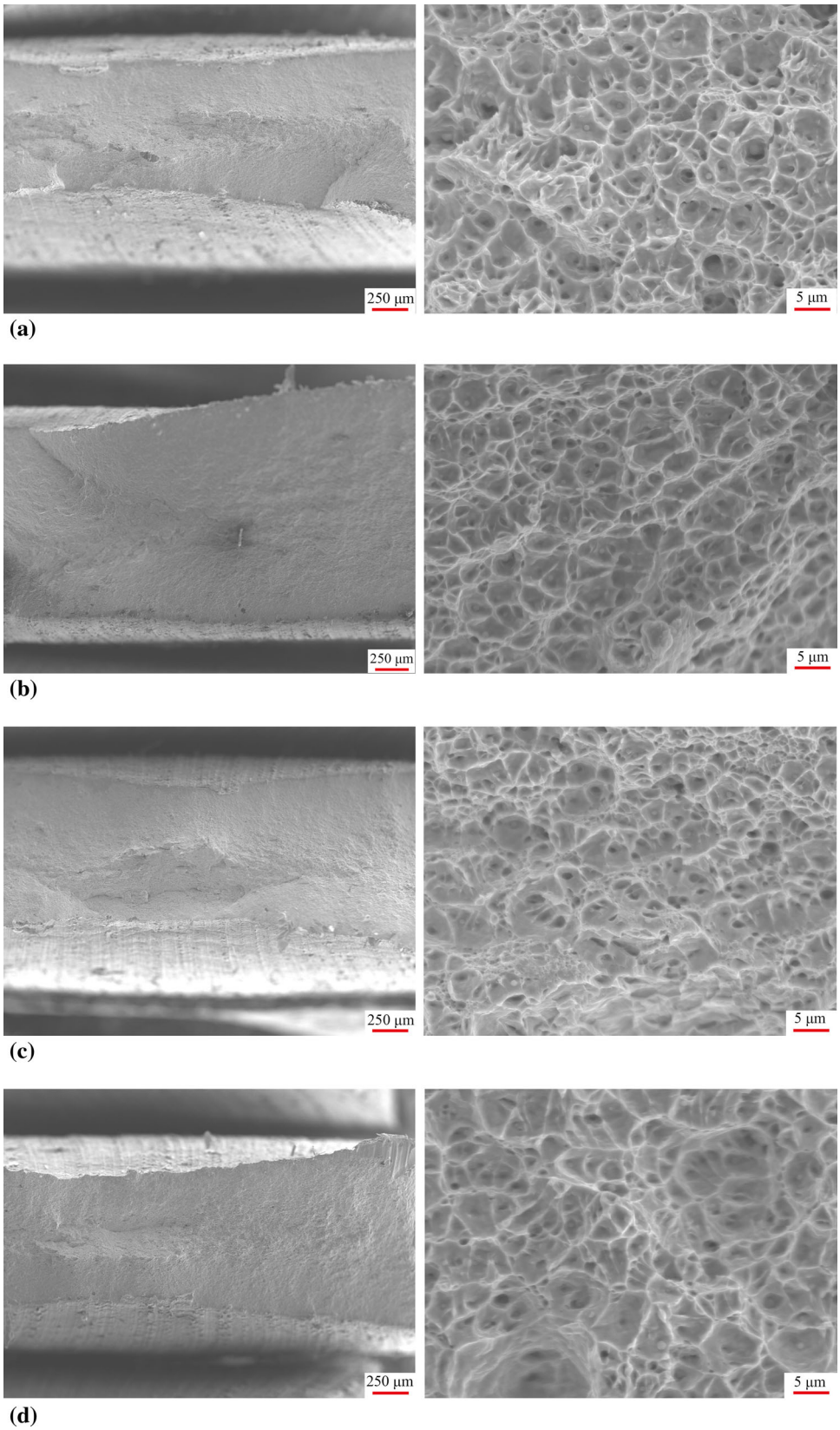

Fig. 12 Fractograph morphology of tensile samples. (a) Horizontal sample of conventional GMA-AM. (b) Vertical sample of conventional GMA-AM. (c) Horizontal sample of double-electrode GMA-AM with bypass arc. (d) Vertical sample of double-electrode GMA-AM with bypass arc

Acknowledgments

This work was supported by National Natural Science Foundation of China, No. 51805266 and 51905273.

References

1. T. DebRoy, H. Wei, J. Zuback, T. Mukherjee, J. Elmer, J. Milewski, A. Beese, A. Wilson-Heid, A. De and W. Zhang, Additive Manufacturing of Metallic Components – Process, Structure and Properties, *Prog. Mater. Sci.*, 2018, **92**, p 112–224
2. A. Bandyopadhyay, Y. Zhang and S. Bose, Recent Developments in Metal Additive Manufacturing, *Curr. Opin. Chem. Eng.*, 2020, **28**, p 96–104
3. J. Xiong, Y. Liu and Z. Yin, Passive Vision Measurement for robust Reconstruction of Molten Pool in Wire and Arc Additive Manufacturing, *Measurement*, 2020, **1531**, p 107407
4. B. Wu, Z. Pan, D. Ding, D. Cuiuri, H. Li, J. Xu and J. Norrish, A Review of the Wire Arc Additive Manufacturing of Metals: Properties, Defects and Quality Improvement, *J. Manuf. Proc.*, 2018, **35**, p 127–138
5. F. Lu, H. Wang, A. Murphy and B. Carlson, Analysis of Energy Flow in Gas Metal Arc Welding Processes through Self-consistent Three-dimensional Process Simulation, *Int. J. Heat Mass. Tran.*, 2014, **68**, p 215–223
6. H. Zhao, G. Zhang, Z. Yin and L. Wu, A 3D Dynamic Analysis of Thermal Behavior During Single-Pass Multi-layer Weld-based Rapid Prototyping, *J. Mater. Process. Technol.*, 2011, **211**, p 488–495
7. J. Spencer, P. Dickens and C. Wykes, Rapid Prototyping of Metal Parts by Three-Dimensional Welding, *Proc. Inst. Mech. Eng. Part B-J. Eng. Manuf.*, 1998, **212**, p 175–182
8. Y. Zhang, Y. Chen, P. Li and A. Male, Weld Deposition-based Rapid Prototyping: A Preliminary Study, *J. Mater. Process Technol.*, 2003, **135**, p 347–357
9. D. Ding, Z. Pan, D. Cuiuri and H. Li, A Practical Path Planning Methodology for Wire and Arc Additive Manufacturing of Thin-walled Structures, *Robot. Com. Int. Manuf.*, 2015, **34**, p 8–19
10. Y. Li, Y. Sun, Q. Han, G. Zhang and I. Horváth, Enhanced Beads Overlapping Model for Wire and Arc Additive Manufacturing of Multi-layer Multi-bead Metallic Parts, *J. Mater. Process. Technol.*, 2018, **252**, p 838–848
11. J. Xiong, M. Shi, Y. Liu and Z. Yin, Virtual Binocular Vision Sensing and Control of Molten Pool Width for Gas Metal Arc Additive Manufactured Thin-walled Components, *Addit. Manuf.*, 2020, **33**, p 101121
12. X. Bai, H. Zhang and G. Wang, Electromagnetically Confined Weld-based Additive Manufacturing, *Procedia CIRP*, 2013, **6**, p 515–520
13. Y. Song and S. Park, Experimental Investigations into Rapid Prototyping of Composites by Novel Hybrid Deposition Process, *J. Mater. Process. Technol.*, 2006, **171**, p 35–40
14. D. Yang, C. He and G. Zhang, Forming Characteristics of Thin-wall Steel Parts by Double Electrode GMAW based Additive Manufacturing, *J. Mater. Process. Technol.*, 2016, **227**, p 153–160
15. J. Huang, W. Yuan, S. Yu, L. Zhang, X. Yu and D. Fan, Droplet Transfer Behavior in Bypass-Coupled Wire Arc Additive Manufacturing, *J. Manuf. Proc.*, 2020, **49**, p 397–412
16. S. Oomen-Hurst, M. Abad, M. Khanna and S. Veldhuis, Comparative Wear Behavior Studies of Coated Inserts during Milling of NiCrMoV Steel, *Tribol. Int.*, 2012, **53**, p 115–123
17. T. Rodrigues, V. Duarte, J. Avila, T. Santos, R. Miranda and J. Oliveira, Wire and Arc Additive Manufacturing of HSLA Steel: Effect of Thermal Cycles on Microstructure and Mechanical Properties, *Addit. Manuf.*, 2019, **27**, p 440–450
18. P. Dirsu, S. Ganguly, A. Mehmanparast, F. Martina and S. Williams, Analysis of Fracture Toughness Properties of Wire + Arc Additive Manufactured High Strength Low Alloy Structural Steel Components, *Mater. Sci. Eng. A*, 2019, **765**, p 138285
19. A. Nemani, M. Ghaffari and A. Nasiri, Comparison of Microstructural Characteristics and Mechanical Properties of Shipbuilding Steel Plates Fabricated by Conventional Rolling Versus Wire Arc Additive Manufacturing, *Addit. Manuf.*, 2020, **32**, p 101056
20. D. Yang, G. Wang and G. Zhang, A Comparative Study of GMAW- and DE-GMAW-based Additive Manufacturing Techniques: Thermal Behavior of the Deposition Process for Thin-walled Parts, *Int. J. Adv. Manuf. Technol.*, 2017, **91**, p 2175–2184
21. D. Li, Research on Cold Crack Criterion of 10Ni5CrMoV Steel Welding Structure with Large Restraint and Development of Austenitic Welding Wire. PhD Thesis. Harbin Institute of Technology, China, 2019. (**In Chinese**)
22. H. Zhang, G. Zhang, J. Wang and L. Wu, Effect of Thermal Cycles of DSAW on Microstructure in Low Alloy High Strength Steel, *Trans. China Weld. Inst.*, 2007, **28**(10), p 81–84. (**In Chinese**)